Kinetic oxidation of antipyrine in heat-activated persulfate

Chaoqun Tan[a], Naiyun Gao[a,*], Yang Deng[b], Lei Li[a], Jing Deng[a], Shiqing Zhou[a]

[a]State Key Laboratory of Pollution Control and Resource Reuse, Tongji University, 1239 Siping Road, Shanghai 200092, China
Tel. +86 021 65982691; email: gaonaiyun1@126.com
[b]Department of Earth and Environmental Studies, Montclair State University, Montclair 07043, NJ, USA

ABSTRACT

The kinetic oxidation of antipyrine by activated persulfate oxidation was investigated. The reaction kinetic rates under different temperature (T, 40–70℃), initial persulfate concentration ($[PS]_0$), and initial antipyrine concentration ($[AP]_0$) were examined in batch experiments. The results show that higher temperature, higher persulfate concentration, and lower initial antipyrine favored antipyrine degradation. A deep investigation into the reaction order obtained a more accurate kinetics rate equation ($-d[AP]/dt = 0.34 [PS]_0 [AP]$) with the limits of the experimental conditions applied here. The removal of antipyrine in 120 min was 54.3% at pH 4.5, and antipyrine degradation at different pH followed the order: pH 4.5 > pH 11.0 > pH 7.0 > pH 9.5. The persulfate disappearance fits pseudo-first-order kinetics well, the calculated disappearance rate of persulfate (k_{obs-PS}) was $2.33 \pm 0.23 \times 10^{-4} min^{-1}$ at 60℃. Although 71.4% of initial antipyrine was degraded at 60℃, only 12.5% of initial antipyrine was mineralized. At last, norantipyrine and 5-pyrazolidinone-3-methyl-1-phenyl were identified to be the degradation products of antipyrine in heat activated persulfate system for the first time, and the degradation pathway of antipyrine was also tentatively proposed.

Keywords: Antipyrine; Degradation products; Heat; Kinetics; Persulfate
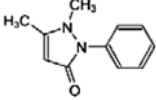
1. Introduction

The occurrence of pharmaceuticals and personal care products (PPCPs) in natural water bodies has been recognized as an emerging issue in environmental quality. Some PPCPs have been reported at a μg/L range level [1–3]. As a result of their non-biodegradability, many PPCPs have been frequently detected in raw water and finished water in drinking water treatment plants, and secondary effluent in wastewater treatment plants [4,5]. Antipyrine (also known as Phenazone, AP), a commonly used analgesic,

represents one of the most commonly identified pharmaceuticals in the environment [6–8]. Antipyrine is among the pharmaceuticals of highest environmental persistence [9], while the ecotoxicity of antipyrine is still largely unknown. Basic physical and chemical properties of antipyrine are shown in Table 1. Antipyrine appears to be very refractory during traditional treatment. For example, only up to 30% of antipyrine was accomplished in conventional wastewater treatment plants [10]. And chlorination with a dose of 0.4 mg/L chlorine only removed 48% of an initial 50 μg/L antipyrine in tap water [11].

*Corresponding author.

Table 1
Physical and chemical characteristics of AP

Name	Molecular structure	Formula	Molecular weight	Water solubility g/L, 20℃	$\log K_{ow}$	Density, g/cm³	Melting point, ℃	Boiling point, ℃
Antipyrine		$C_{11}H_{12}N_2O$	188.23	1,000	0.38	1.07	110–113	319

In-situ chemical oxidation (ISCO) is becoming a promising alternative for traditional environmental remediation technologies. During ISCO, reactive oxidizing agents such as permanganate, ozone, hydrogen peroxide, and persulfate salts are injected into groundwater or soil for the purpose of rapid destruction of subsurface contaminants of concern. Among the ISCO oxidants, persulfate ($S_2O_8^{2-}$, PS) has been paid more and more attention to because sulfate radicals ($SO_4^{\cdot-}$), a much more powerful oxidant, may be produced through activation of $S_2O_8^{2-}$ using certain methods such as ultraviolet (UV) light, metals, or heat, as follows (Eqs. (1)–(3)) [12–16].

$$S_2O_8^{2-} + UV \rightarrow 2SO_4^{\cdot-} \tag{1}$$

$$S_2O_8^{2-} + Me^{n+} \rightarrow 2SO_4^{\cdot-} + Me^{(n+1)+} + SO_4^{2-} \tag{2}$$

$$S_2O_8^{2-} + heat \rightarrow 2SO_4^{\cdot-} \tag{3}$$

However, UV or metal activation is highly restricted, because UV cannot make an effective transmission in a subsurface environment [17], and much metal sludge will be produced after metal activation to reduce local hydraulic conductivity [18]. Heat is the most favored activation mode suitable for ISCO [19,20]. Furthermore, a high temperature in injection sites is more effective than UV or metal activation in terms of production of $SO_4^{\cdot-}$, so that higher reaction rates are accomplished, shorter reaction time is required, and less chemical agents are needed [21–23].

The objective of this study was to characterize the degradation of antipyrine in a heat activated persulfate system. Kinetics tests were conducted to study the antipyrine degradation behaviors under different persulfate doses, initial antipyrine concentrations, and temperatures. Both decomposition and mineralization of antipyrine were evaluated. Gas chromatography–mass spectrometry–mass spectrometry (GC–MS–MS) techniques were used to determine the antipyrine oxidation products in water, thus revealing the degradation pathway of antipyrine.

2. Experimental

2.1. Chemicals

All chemicals were at least analytical grade, except as noted. All the solutions were prepared using the ultrapure water produced from a Milli-Q Academic water purification system. Antipyrine, methanol, and *n*-hexane (Chromatograph grade, ≥99.9%) were purchased from Sigma–Aldrich. Sodium persulfate ($Na_2S_2O_8$, purity ≥99.5%), ferrous ammonium sulfate hexahydrate ($Fe(NH_4)_2(SO_4)_2 \cdot 6H_2O$, purity ≥99.7%), ammonium thiocyanate (NH_4SCN, purity ≥99.9%), sodium bicarbonate ($NaHCO_3$, purity ≥99.5%), and sodium sulfite (Na_2SO_3, purity ≥99.9%) were purchased from Sinopharm Chemical Reagent Co., China.

2.2. Experimental procedure

All the tests were conducted in 250-mL culture bottles containing 200 mL antipyrine solution. The reactors were installed in a shaking bed with water bath (SHZ-B immersion oscillator registration) that could control the reaction temperature at a desirable level. A rapid shaking ensured a complete solution mixing state. Sodium persulfate stock solution (0.05 M) was prepared 30 min prior to reaction in case that persulfate decayed before use. The oxidation reaction was initiated once appropriate volumes of the persulfate stock solution were added to the reactors. At each sampling time, 0.8 mL sample was collected and stored in 1.5 mL sample bottles for further sample analysis. The sample bottles were pre-filled with 0.2 mL ethanol that could quench the oxidation caused by any residual persulfate. Another 20 mL sample for total organic carbon (TOC) analysis was collected in 40 mL sample bottles that were pre-filled with 20 mL sodium sulfite (0.5 M) to quench any residual persulfate-induced oxidation. All the tests were performed at least in triplicate. Symbols and error bars in figures represent the mean values and standard deviations of the data obtained, respectively.

2.3. Chemical analysis

Antipyrine was measured using a high-performance liquid chromatograph (HPLC) (Waters 2010, USA) equipped with a Symmetry C18 column (dimensions $250\,mm \times 4.6\,mm$, $5\,\mu m$, Waters, USA) and a UV detector (Waters 2489) set at 260 nm. The mobile phase was a mixture of Milli-Q water and HPLC-grade methanol (v:v = 20:80) at a flow rate of 0.8 mL/min [24]. TOC was measured by a total organic carbon analyzer (TOC-L, CPH CN200, Shimadzu). The oxidation by-products were identified by GC (Thermo Trace GC Ultra, USA)-MS/MS (Thermo TSQ Quantum XLS, USA). The GC was equipped with a TR-5MS capillary column $30\,m \times 0.25\,mm \times 25\,\mu m$. The carrier gas was high purity helium (>99.999%, Chunyu Corp., China) at a pressure of 90 kPa. The injection port was operated at a splitless mode with a controlled temperature of 250°C. The oven temperature program was initially set at 50°C for 1 min, then increased at a rate of 10–250°C/min, and finally maintained at 250°C for 5 min. The MS/MS parameters were determined using the method reported in a previous study [11]. Persulfate concentration was measured using a UV–Vis spectrophotometer (HACH DR5000) equipped with quartz cuvettes of 1 cm light path [25]. Statistical analysis was performed using Origin 8.0. Linear regressions were performed to determine the first-order rate constants for the antipyrine degradation.

3. Results and discussion

3.1. Kinetic parameters

Fig. 1 presents the antipyrine degradation with time in the presence of persulfate under different temperatures (30–70°C). The results show that antipyrine degradation was highly temperature dependent. Generally, higher temperature activation led to faster antipyrine degradation. Complete removal was observed at 40 min when the reaction carried out at 70°C. At 30°C, the degradation of antipyrine was almost marginal, thus suggesting that persulfate alone without activation can hardly oxidize antipyrine in 2 h. When the reaction temperature was increased over 40°C, the antipyrine degradation was significant. At 40~70°C, the degradation kinetics experimental data well follow pseudo-first-order reaction pattern ($R^2 > 0.95$). Therefore, the overall rate law for the antipyrine degradation can be expressed as Eq. (4):

$$-d[AP]/dt = k_{obs}[AP] \tag{4}$$

where k_{obs} is the pseudo-first-order rate constant, and [AP] is the mole concentration of antipyrine at any
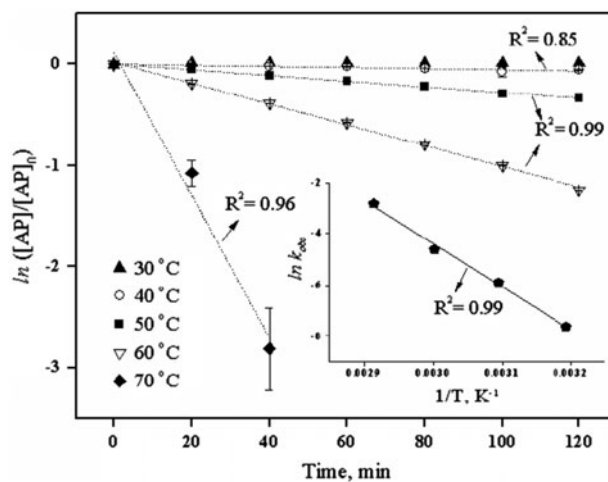

Fig. 1. Pesudo-first-order disappearance of antipyrine at different temperatures. Inset: plot of $\ln k_{obs}$ vs $1/T$ for E_a estimation using the Arrhenius equation. Experimental conditions: initial pH = 7.1, unbuffered; $[Antipyrine]_0 = 0.0265\,mM$; $[Na_2S_2O_8]_0 = 1.855\,mM$. $[Na_2S_2O_8]_0/[Antipyrine]_0 = 70:1$.

specific time. For an initial antipyrine concentration of 0.0265 mM, the pseudo-first-order rate constants were 0.0005, 0.0027, 0.0092, and $0.0584\,min^{-1}$ when the temperature was 40, 50, 60, and 70°C, respectively.

As shown in the inset of Fig. 1, the pseudo-first-order rate constants and corresponding reaction temperatures well fit the Arrhenius equation ($R^2 = 0.99$, Eq. (5)).

$$\ln k_{obs} = \ln A - E_a/RT \tag{5}$$

where A is the frequency factor, E_a is the activation energy, R is the universal gas constant (8.314 J/mol K), and T is the absolute temperature (K). The calculated Arrhenius constant A was approximately $8.93 \pm 0.67 \times 10^{19}\,min^{-1}$, and the activation energy E_a was $139.5 \pm 9.7\,kJ/mol$. The estimated E_a was slightly lower than the one reported by Ghauch and Tuqan [26,27] during the degradation of ibuprofen by heat-activated persulfate oxidation ($E_a = 168.4 \pm 9.5\,kJ/mol$), but greater than the degradation of bisoprolol ($E_a = 119.4 \pm 10.8\,kJ/mol$).

3.2. Effect of the persulfate dose

Effect of the persulfate dose on the degradation kinetics of antipyrine is shown in Fig. 2. The different persulfate doses were achieved by fixing the initial antipyrine concentration ($[AP]_0$) at 0.0265 mM and adding persulfate at different doses ($[PS]_0$) of 0, 0.27, 1.06, 1.86, and 2.65 mM at 60°C. The temperature of 60°C in all kinetics study was selected because the
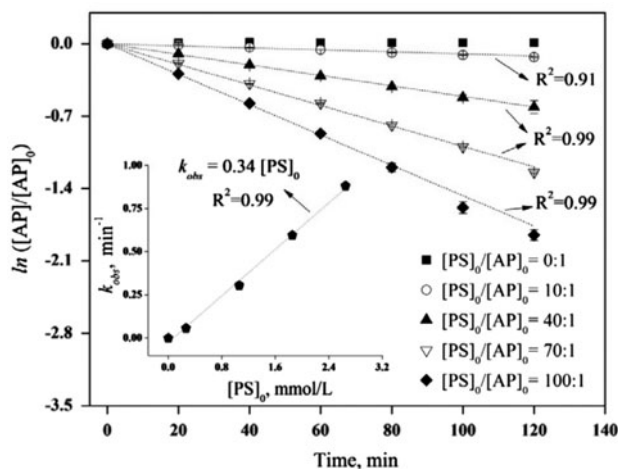
Fig. 2. Pesudo-first-order disappearance of antipyrine at different persulfate dosage. Inset: plot of k_{obs} vs persulfate dosage. Experimental conditions: unbuffered; [antipyrine]$_0$ = 0.0265 mM; [Na$_2$S$_2$O$_8$]$_0$ = 0.00–2.650 mM; T = 60°C.
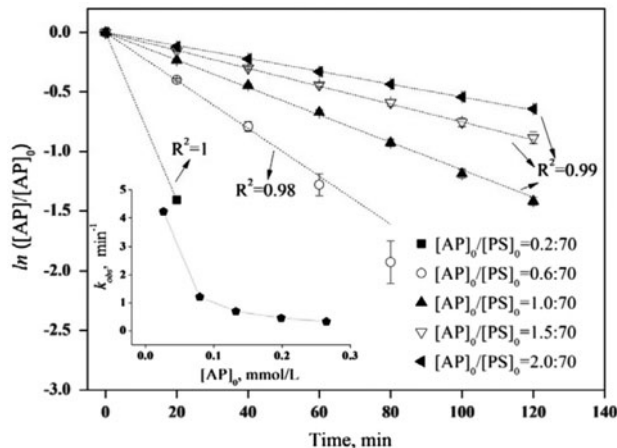

Fig. 3. Pesudo-first-order disappearance of antipyrine at different initial antipyrine concentration. Inset: plot of k_{obs} vs antipyrine concentration. Experimental conditions: unbuffered; [AP]$_0$ = 0.005–0.053 mM; [Na$_2$S$_2$O$_8$]$_0$ = 1.86 mM; T = 60°C.

removal of antipyrine by heat activated persulfate system at 60°C was 73% at 2 h, the oxidation rate and removal are suitable for studying the degradation product and effect of concentration. For any particular persulfate dose, the antipyrine degradation followed a first-order reaction pattern. Therefore, the antipyrine degradation rate could be written as Eq. (4). With the increase of [PS]$_0$:[AP]$_0$ from 0:1 to 100:1, the observed constant (k_{obs}) was increased from 0 to 0.88 min^{-1}. Furthermore, k_{obs} exhibited a linear relationship with [PS]$_0$ with a slope of 0.34 (R^2 = 0.99). Therefore, k_{obs} could be expressed as a function of [PS]$_0$, as Eq. (6).

$$K_{obs} = 0.34\,[PS]_0 \tag{6}$$

Therefore, Eq. (6) can be re-written as Eq. (7).

$$-d[AP]/dt = 0.34\,[PS]_0[AP] \tag{7}$$

Similar results were reported for heat-activated persulfate oxidation of diuron [17] and methyl tert-butyl ether (MTBE) [28], with their respective degradation rate equations of $-d[\text{Diuron}]/dt = 0.69$ [PS]$_0$ [Diuron] and $-d[\text{MTBE}]/dt = 3.67$ [PS]$_0$ [MTBE].

3.3. Effect of initial antipyrine concentration

Effect of the initial antipyrine concentration on heat-activated persulfate oxidation of antipyrine is presented in Fig. 3. All the tests were run at a fixed persulfate dose of 1.86 mM. Under different [AP]$_0$:[PS]$_0$ (0.2:70–2:70), the decomposition exhibited pseudo-first-order kinetics behaviors well ($R^2 \geqslant 0.99$).

Typically, higher initial antipyrine concentrations led to slower antipyrine degradation. This because that the amount of sulfate radicals generated was constant at a fixed persulfate dose and under certain conditions. The fraction of antipyrine decomposed by sulfate radicals was less at a high [AP]$_0$ than at a low one. When the initial antipyrine increased from 0.005 to 0.053 mM, the pseudo-first-order rate constants (k_{obs}) decreased from 4.22 to 0.33 min^{-1}. The pseudo-first-order rate constant (k_{obs}) herein was greater than those in hydroxyl radical-induced oxidation of antipyrine. Klamerth et al. [29] observed the k_{obs} of 0.007 min^{-1} using a UV/H$_2$O$_2$ system at a H$_2$O$_2$ dose of 0.147 μM and an initial antipyrine 0.53 μM. Garcia et al. [30] reported the k_{obs} of 0.022 min^{-1} in a UV/TiO$_2$ system with TiO$_2$ = 0.062 mM and an initial antipyrine concentration of 0.53 μM.

3.4. Effect of pH

The effect of solution pH (4.5~11.0) on antipyrine degradation in heat-activated persulfate system is shown in Fig. 4. The removal of antipyrine in 120 min was 54.3% at pH 4.5, and it decreased to 39.4% when pH increased to pH 7.0, then further decreased to 35.8% when pH was 9.5, which was the lowest removal in selected pH ranges. However, about 54.8% of initial antipyrine was degraded at pH 11.0, which was the highest removal in the experimental pH range. The removal of antipyrine at acid pH was caused by the generated SO_4^- by heat activated persulfate according to Eq. (3). While, the removal of antipyrine decreased as pH increased from 4.5 to 9.5.
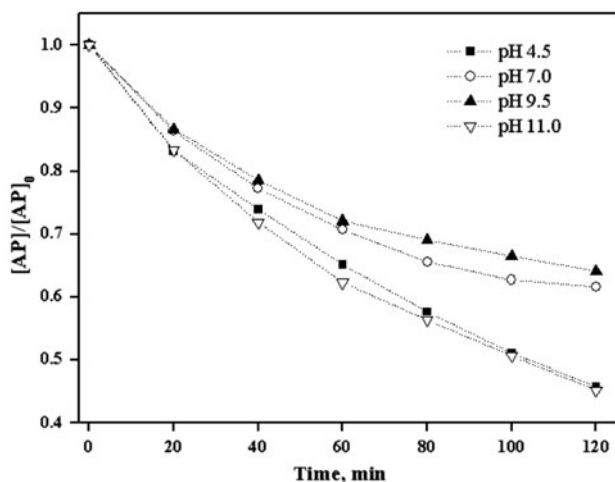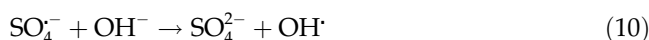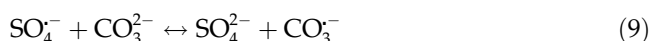
Fig. 4. Removal of antipyrine at different buffered pH. Experimental conditions: buffered; $[AP]_0 = 0.0265$ mM; $[Na_2S_2O_8]_0 = 1.86$ mM; $T = 60$℃.

This result was mostly caused by the alkalinity effect in system when pH increased because the culture bottles in our study were open to the air. The alkalinity in system increased as pH increased because the CO_2 in air and produced from mineralization would transform to CO_3^{2-} or HCO_3^-. And CO_3^{2-} or HCO_3^- are well-known radical scavengers that could compete with antipyrine for radicals produced in system as follows [31] (Eq. (8–10)):

$$SO_4^{\cdot-} + HCO_3^- \leftrightarrow SO_4^{2-} + HCO_3^{\cdot} \tag{8}$$

$$SO_4^{\cdot-} + CO_3^{2-} \leftrightarrow SO_4^{2-} + CO_3^{\cdot-} \tag{9}$$

$$SO_4^{\cdot-} + OH^- \rightarrow SO_4^{2-} + OH^{\cdot} \tag{10}$$

Similar finding was also reported by Deng and Ezyske [32] who applied the sulfate radical-advanced oxidation process for treatment of landfill leachate, they reported 37 and 25% COD removal at pH 4.5 and 7.0, respectively, because the alkalinity in system increased. On the other hand, as pH increased to pH 11.0, great amount of OH^- in solution could activate $SO_4^{\cdot-}$ to $OH^{\cdot}$. The $OH^{\cdot}$ was more powerful to degrade antipyrine, resulting in obvious increase of degradation efficiency.

3.5. Persulfate decay and antipyrine mineralization

The longevity of persulfate is critically important in practice, because certain time is needed for persulfate to transport from an injection well to a contamination zone during ISCO. The persulfate decay at 60℃ is shown in Fig. 5. The persulfate concentration gradually dropped from 1.89 (450) to 1.83 mM (435 ppm) within the first 2 h. The persulfate decay well fit with the first pseudo-first-order kinetics model with an observed rate constant of 2.33 $(\pm 0.23) \times 10^{-4}$ min^{-1}. This finding was in accordance with previous studies [33,34] that tested the decay rate of persulfate at 60℃. Kolthoff et al. found the persulfate decay rate constant at 3.0×10^{-4} min^{-1} in the presence of 0.1 M NaOH. This slightly greater rate constant might be because NaOH in their study acted as an additional activator to produce excess sulfate radical [35]. Johnson et al. determined a similar $k_{obs\text{-}PS}$ of 2.7×10^{-4} min^{-1} in deionized water.

Antipyrine mineralization was expressed as TOC reduction. Accompanied with the persulfate decay, TOC was also reduced with time, as shown in Fig. 5. After 120 min reaction, the initial TOC of 3.91 decreased to 3.42 ppm, corresponding to a 12.5% overall mineralization. This finding, together with the results reported above, indicate that in this study (60℃, $[PS]_0/[AP]_0 = 70:1$, $[AP]_0 = 0.0265$ mM), approximately 71.4% of initial antipyrine (see from Fig. 1) could be degraded, while only 12.5% of the initial antipyrine could be mineralized within 120 min.

3.6. Degradation pathways of antipyrine supposed

Antipyrine has been broadly used as antitumor [36], antimicrobial [37,38], analgesic [39], or anticancer drugs [40]. Its metabolites in human or animal bodies have been reported in numerous studies [41–43]. In most cases, antipyrine is metabolized by microbial organisms into four major metabolites,
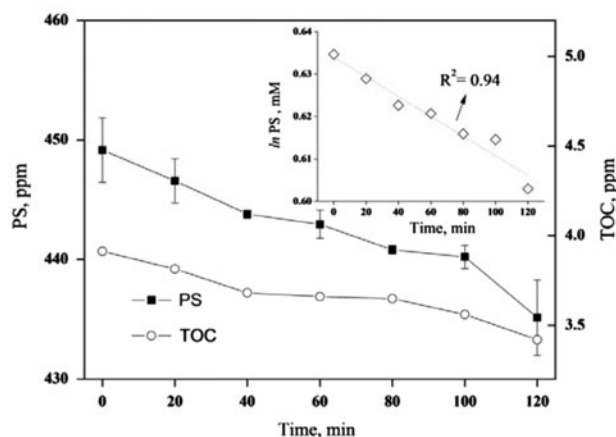

Fig. 5. Persulfate and TOC disappearance vs. time. Inset: plot of $\ln k_{obs\text{-}PS}$ vs time. Experimental conditions: unbuffered; $[AP]_0 = 0.0265$ mM; $[Na_2S_2O_8]_0 = 1.86$ mM; $T = 60$℃.

i.e. 3-hydroxyl-methylantipyrine (HMA), 4-hydroxy-antipyrine (OHA), 4,4′-dihydroxyantipyrine (DOHA), and norantipyrine (NORA). However, about the knowledge on the degradation products of antipyrine during ISCO is limited. In this study, GC–MS–MS showed that none of HMA, OHA, and DOHA was
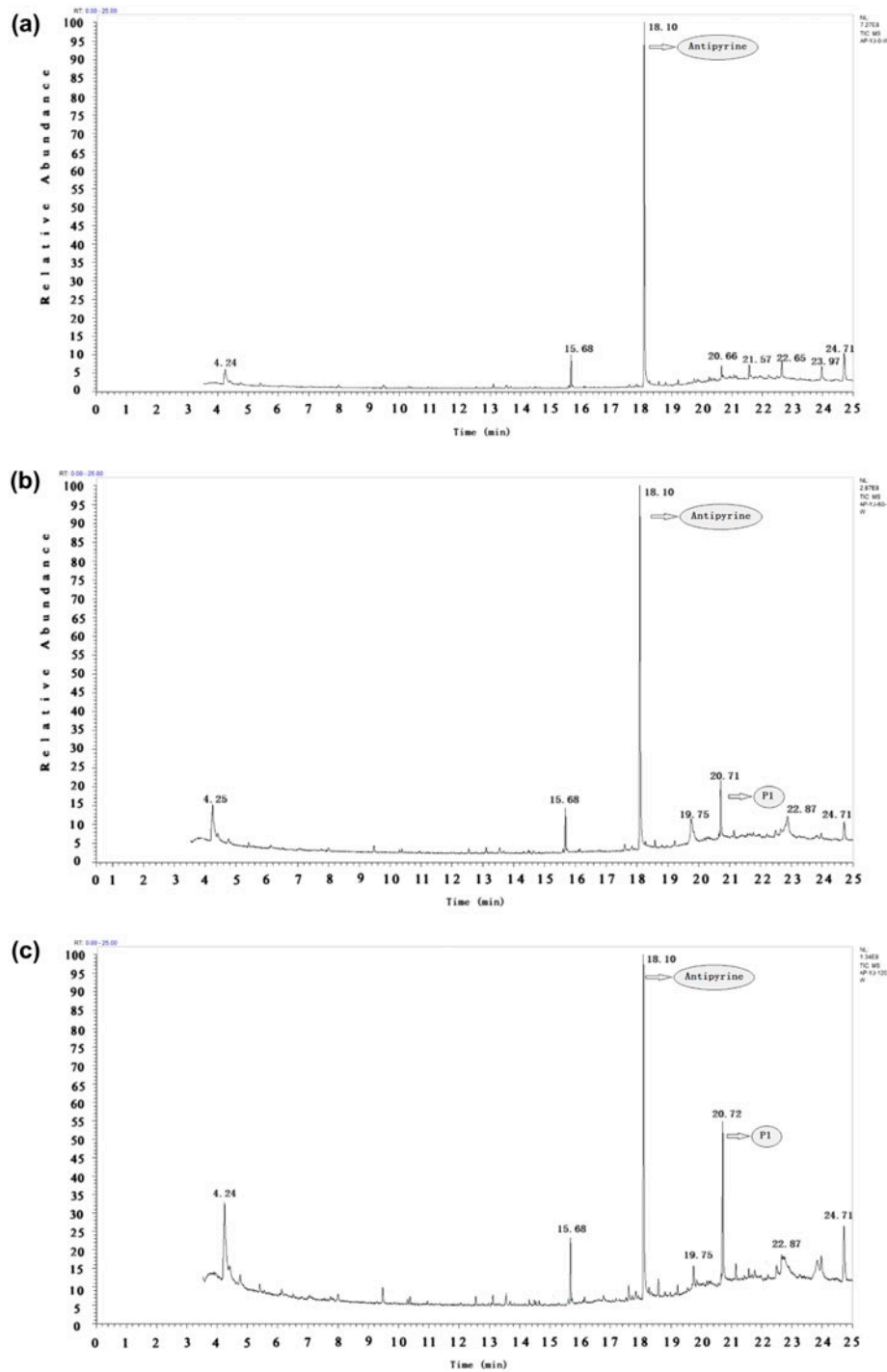

Fig. 6. The chromatograph obtained in test. Experimental conditions: $[AP]_0 = 0.0265$ mM; $[Na_2S_2O_8]_0 = 1.86$ mM; $T = 60$°C. (a) The total ionic chromatograph at 0 min. (b) The total ionic chromatograph at 60 min. (c) The total ionic chromatograph at 120 min. (d) The mass spectrum of P_t searched from the main lib in GC–MSMS. (e) The comparison between mass spectrum obtained in our study at 20.71 min in (c) and mass spectrum of P_t from main lib searched by the main lib in GC–MSMS.
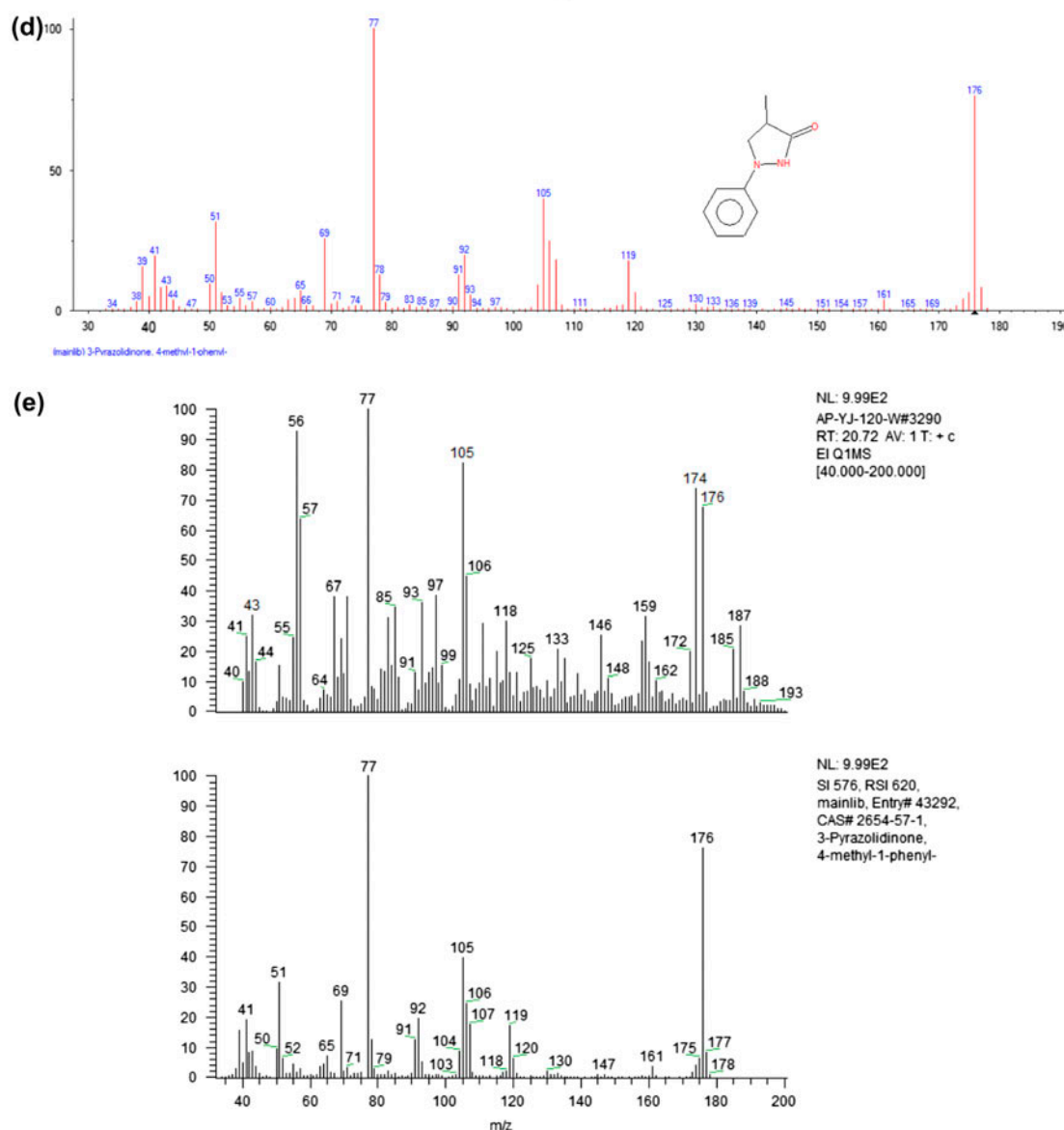
Fig. 6. (*Continued*)

identified (Fig. 6). Instead, $C_{10}H_{10}N_2O$ ($m/z = 174$, it is likely to be NORA) and $C_{10}H_{12}N_2O$ ($m/z = 176$, it is likely to be P_t, 3-pyrazolidinone-4-methyl-1-phenyl) were largely detected. However, the structure of P_t was obviously not corresponding with the structure of antipyrine. Because the C=O band, which was much stable in reaction, was not at its original position. The correct position for C=O should be at C_5 position, while its position in P_t was at C_3 position.

From the structure of AP, NORA, and P_t, we proposed P_1 (P_1, $m/z = 176$, 5-pyrazolidinone-3-methyl-1-phenyl), a geometric isomer of P_t, to be the degradation product of AP. Based on the results

of the GC–MS–MS, the degradation pathway of antipyrine is proposed in Fig. 7. Antipyrine was firstly degraded to be NORA, and further decomposed into P_1 ($m/z = 176$, 5-pyrazolidinone-3-methyl-1-phenyl), a geometric isomer of P_t. In the first step, NORA was formed via direct elimination of the methyl radical located at N_2 instead of C_3. In a similar study, Deng et al. [44] found that the appearance energies for elimination of methyl radical from N_2 position and from C_3 position were 9.59 and 12.42 eV, respectively. In the following step, further degradation would occur by opening the double bond between C_3 and C_4 to transform into P_1.
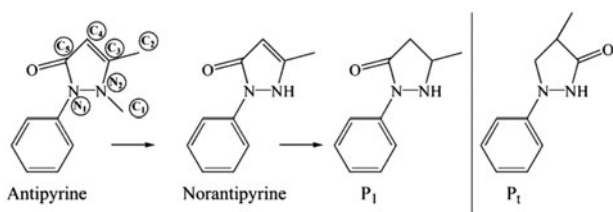
Fig. 7. The proposed antipyrine degradation pathway (Antipyrine → Norantipyrine → P_1). Experimental conditions: unbuffered; $[AP]_0 = 0.0265$ mM; $[Na_2S_2O_8]_0 = 1.86$ mM; $T = 60$ ℃.

4. Conclusions

In this study, kinetics tests were conducted to study heat-activated persulfate oxidation of AP, and GC–MS–MS analysis further revealed the antipyrine degradation pathway. Results show that the sulfate radical-based advanced oxidation could adequately degrade antipyrine in water within a relatively short time, thus implying that the heat-activated persulfate is a potential method to control AP-induced water pollution. However, the antipyrine mineralization was insignificant, thus indicating that the intermediate and final oxidation products of antipyrine were recalcitrant to sulfate radical oxidation.

Acknowledgments

Abbreviations

AP	—	antipyrine
E_0	—	redox potential
E_a	—	the activation energy
ISCO	—	*in situ* chemical oxidation
k_{obs}	—	pseudo-first-order degradation rate
OH·	—	hydroxyl radicals
PPCPs	—	pharmaceuticals and personal care products
PS	—	persulfate
SO_4^-	—	sulfate radicals
P_t	—	5-pyrazolidinone-3-methyl-1-phenyl
P_1	—	5-pyrazolidinone-3-methyl-1-phenyl, a geometric isomer of P_t

References

[1] B. Halling-Sørensen, S.N. Nielsen, P.F. Lanzky, F. Ingerslev, H.C.H. Lutzhøft, S.E. Jørgensen, Occurrence, fate and effects of pharmaceutical substances in the environmental: A review, Chemosphere 36 (1998) 357–393.

[2] O.A.H. Jones, N. Voulvoulis, J.N. Lester, Aquatic environmental assessment of the top 25 english prescription pharmaceuticals, Water Res. 36 (2002) 5013–5022.

[3] J.P. Bound, N. Voulvoulis, Predicted and measured concentration for selected pharmaceuticals in UK rivers: Implications for risk assessment, Water Res. 40 (2006) 2885–2892.

[4] M.J. Benotte, B.A. Trenholm, B.J. Vanderford, J.C. Holady, B.D. Stanford, S.A. Snyder, Pharmaceuticals and endocrine disrupting compounds in US drinking water, Environ. Sci. Technol. 43 (2009) 597–603.

[5] B.J. Vanderford, R.A. Pearson, S.A. Snyder, Analysis of endocrine disruptors and personal care products in water using liquid chromatography/tandem mass spectrometry, Anal. Chem. 75 (2005) 8220–8226.

[6] T. Ternes, M. Bonerz, T. Schmidt, Determination of neutral pharmaceuticals in wastewater and rivers by liquid chromatography electrospray tandem mass spectrometry, J. Chromatogr. A 938 (2001) 175–185.

[7] R. Schmidt, R. Brockmeyer, Occurrence and behavior of expectorants, analgesics, xylometazoline and their metabolites in water and during bank filtration, Vom. Waste 98 (2002) 37–54.

[8] S. Wiegel, A. Aulinger, R. Brockmeyer, H. Harms, J. Loffler, H. Reincke, R. Schmidt, B. Stachel, W.V. Tumpling, A. Wanke, Pharmaceuticals in the river Elbe and its tributaries, Chemosphere 57 (2004) 107–126.

[9] A. Sadezky, D. Loffler, T. Ternes, Report D.01. Proposal of an Environmental Indicator and the Classification System of Pharmaceutical Product Residues for Environmental Management, Knowledge and Need Assessment on Pharmaceutical Products in Environmental Waters, Koblenz, 2008.

[10] S. Zuehlke, U. Duennbier, B. Lesjean, R. Gnirss, H. Buisson, Long-term comparison of trace organics removal performances between conventional and membrane activated sludge processes, Water Environ. Res. 78 (2006) 2480–2486.

[11] R. Rodil, J.B. Quintana, R. Cela, Transformation of phenazone-type drugs during chlorination, Water Res. 46 (2012) 2457–2468.

[12] G.P. Anipsitakis, D.D. Dionysiou, Radical generation by the interaction of transition metals with common oxidants, Environ. Sci. Technol. 38 (2004) 3705–3712.

[13] C.J. Liang, C.J. Bruell, M.C. Marley, K.L. Sperry, Persulfate oxidation for *in situ* remediation of TCE. I. activated by ferrous ion with and without a persulfate-thiosulfate redox couple, Chemosphere 55 (2004) 1213–1223.

[14] C.J. Liang, Z.S. Wang, C.J. Bruell, Influence of pH on persulfate oxidation of TCE at ambient temperatures, Chemosphere 66 (2007) 106–133.

[15] W.K. Wilmarth, A. Haim, Mechanisms of oxidation by peroxydisulfate ion, in: J.O. Edwards (Ed.), Peroxide Reaction Mechanisms, Interscience, New York, NY, 1962, pp. 175–225.

[16] P. Neta, V. Madhavan, H. Zemel, R.W. Fessenden, Rate constants and mechanism of reaction of sulfate radical anion with aromatic compounds, J. Am. Chem. Soc. 99 (1977) 163–164.

[17] C.Q. Tan, N.Y. Gao, Y. Deng, N. An, J. Deng, Heat actitivated persulfate oxidation of diuron in water, Chem. Eng. J. 203 (2012) 294–300.

[18] C.Q. Tan, N.Y. Gao, W.H. Chu, C. Li, M.R. Templeton, Degradation of diuron by persulfate activated with ferrous ion, Sep. Purif. Technol. 95 (2012) 44–48.

[19] V.C. Mora, J.A. Rosso, G.C.L. Roux, D.O. Martire, M.C. Gonzalez, Thermally activated peroxydisulfate in the presence of additives: A clean method for the degradation of pollutants, Chemosphere 75 (2009) 1405–1409.

[20] K.C. Huang, Z.Q. Zhao, G.E. Hoag, A. Dahmani, P.A. Block, Degradation of volatile organic compounds with thermally activated persulfate oxidation, Chemosphere 61 (2005) 551–560.

[21] X.G. Gu, S.G. Lu, L. Li, Z.F. Qiu, Q. Sui, K.F. Lin, Q.S. Luo, Oxidation of 1,1,1-trichloroethane stimulated by thermally activated persulfate, Ind. Eng. Chem. Res. 50 (2011) 11029–11036.

[22] C.J. Liang, H.W. Su, Identification of sulfate and hydroxyl radicals in thermally activated persulfate, Ind. Eng. Chem. Res. 48 (2009) 5558–5562.

[23] C.J. Liang, C.J. Bruell, Thermally activated persulfate oxidation of trichloethylene: Experimental investigation of reaction orders, Ind. Eng. Chem. Res. 47 (2008) 2912–2918.

[24] S.A.J. Coolen, T. Ligor, M.V. Lieshout, F.A. Huf, Determination of phenolic derivatives of antipyrine in plasma with solid-phase extraction and high-performance liquid chromatography-atmospheric-pressure chemical ionization mass spectrometry, J. Chromatogr. B 732 (1999) 103–113.

[25] C.J. Liang, C.F. Huang, N. Mohanty, R.M. Kurakalva, A rapid spectrophotometric determination of persulfate anion in ISCO, Chemosphere 73 (2008) 1540–1543.

[26] A. Ghauch, A.M. Tuqan, N. Kibbi, Ibuprofen removal by heated persulfate in aqueous solution: A kinetic, Chem. Eng. J. 197 (2012) 483–492.

[27] A. Ghauch, A.M. Tuqan, Oxidation of bisoprolol in heated persulfate/H2O systems: Kinetics and products, Chem. Eng. J. 183 (2012) 162–171.

[28] K.C. Huang, R.A. Couttenye, G.E. Hoag, Kinetics of heat-assisted persulfate oxidation of methyl tert-butyl ether (MTBE), Chemosphere 49 (2002) 413–420.

[29] N. Klamerth, L. Rizzo, S. Malato, M.I. Maldonado, A. Aguera, A.R.F. Alba, Degradation of fifteen emerging contaminants at ug/L concentrations by mild solar phtot-Fenton in MWTP effluents, Water Res. 44 (2010) 545–554.

[30] N.M. Garcia, M.I. Maldonado, J.M. Coronado, S. Malato, Degradation study of 15 emerging contaminants at low concentration by immobilized TiO2 in a pilot plant, Catal. Today 115 (2010) 107–113.

[31] L.R. Bennedsen, J. Muff, E.G. Sogaard, Influence of chloride and carbonates on the reactivity of activated persulfate, Chemosphere 86 (2012) 1092–1097.

[32] Y. Deng, C.M. Ezyske, Sulfate radical-advanced oxidation process (SR-AOP) simultaneous removal of refractory organic contaminats and ammonia in landfill leachate, Water Res. 45 (2011) 6189–6194.

[33] I.M. Kolthoff, I.K. Miller, The chemistry of persulfate. I. The kinetics and mechanism of the decomposition of the persulfate ion in aqueous medium, J. Am. Chem. Soc. 73 (1951) 3055–3059.

[34] R.L. Johnson, P.G. Tratnyek, R.O. Johnson, Persulfate persistence under thermal activation conditions, Environ. Sci. Technol. 42 (2008) 9350–9356.

[35] O.S. Furman, A.L. Teel, R.J. Watts, Mechanism of base activation of persulfate, Environ. Sci. Technol. 44 (2010) 6423–6428.

[36] E. Radzikowska, K. Onish, E. Chojak, Prospective assessment of cancer incidence and antipyrine metabolism, Eur. J. Cancer 31A (1995) 1077–1077.

[37] S. Bondock, R. Rabie, H.A. Etman, A.A. Fadda, Synthesis and antimicrobial activity of some new hetercycles incorporating antipyrine moiety, Eur. J. Med. Chem. 43 (2008) 2122–2129.

[38] N.V. Bashkatova, E.I. Korotkova, Y.A. Karbainov, A.Y. Yagovkin, A.A. Bakibaev, Electrochemical, quantum-chemical and antioxidant properties of antipyrine and its derivatives, J. Pharm. Biomed. Anal. 37 (2005) 1143–1147.

[39] Y. Valcarcel, S.G. Alonso, J.L.R. Gil, R.M. Maroto, A. Gil, M. Catala, Analysis of the presence of cardiovascular and analgestic/anti-inflammatory/antipyretic pharmaceuticals in river – And drinking water of the Madrid region in Spain, Chemosphere 82 (2011) 1062–1071.

[40] M.G. Donelli, M. Zucchetti, E. Munzone, M. Dlncalci, A. Crosignani, Pharmacokinetics of anticancer agents in patients with inpaired liver function, Eur. J. Cancer 34 (1998) 33–36.

[41] J.C. Rhodes, S.T. Hall, J.B. Houston, Inhibition of antipyrine metabolite formation in rats in vivo, Xenobiotica 14 (1984) 677–686.

[42] M. Danhof, E.De. Groot-Van, D.D. Breimer, Assay of antipyrine and its primary metabolites in plasma, saliva and urine by high-performance liquid chromatography and some preliminary results in man, Pharmacology 18 (1979) 210–213.

[43] I. Velic, M. Metzler, H.G. Hege, J. Weymann, Seperation and indentification of phase I and phase II [14C] antipyrine metabolites in rat and dog urine, J. Chromatogr. 666 (1995) 139–147.

[44] L.L. Deng, L.D. Zhang, H.J. Guo, L.Y. Jia, Y. Pan, H. Yin, F. Qi, VUV photo-induced ionization/dissociation of antipyrine and propyphenazone: Mass spectrometric and theoretical insights, J. Mass Spectrom. 45 (2010) 734–739.